THEORETICAL AND EXPERIMENTAL INVESTIGATIONS ON THE PHOTO-THERMAL EFFECT OF GOLD NANORODS IRRADIATED BY FEMTOSECOND AND NANOSECOND LASER

by

Dong LI[a], Penghui ZHAO[a], Jing FENG[a], Linzhuang XING[a], Bin CHEN[a*], and Dingying LIAO[b,c*]

[a] State Key Laboratory of Multi-Phase Flow in Power Engineering, Xi 'an Jiaotong University, Xi 'an, Shaanxi, China
[b] Department of Ophthalmology, The Second Affiliated Hospital of Xi 'an Jiaotong University, Xi 'an, Shaanxi, China
[c] Department of Ophthalmology, Peking University Shenzhen Hospital, Shenzhen, China

Original scientific paper
https://doi.org/10.2298/TSCI210828327L

Nanoparticle mediated laser induced breakdown can be used for Nanoparticle synthesis, cell nanosurgery and laser induced breakdown spectroscopy. To investigate the photo-thermal conversion of gold nanoparticles during pulsed laser irradiation, the electron-phonon two temperature model was established in this study. The impact of laser energy density and pulse width on the thermal conversion and morphology change of gold nanorods were investigated and compared with experimental observations. The results show that the melting threshold of gold nanorods under nanosecond laser irradiation is about twenty times that of femtosecond laser irradiation. The mechanisms of nanorod fragmentation are different between femto and nanosecond laser irradiation: particle melting is more likely to occur in nanosecond laser irradiation, while the Coulomb explosion is highly likely to occur in femtosecond laser irradiation.

Key words: *laser induced optical breakdown, photo-thermal effect, electron-phonon-two-temperature model, gold nanorods*

Introduction

The strong interaction between ultrashort pulsed lasers and gold nanoparticles (NP) has vast applications in many fields, such as photonics, electronics, chemistry, medicine and biology. Gold NP, gold nanospheres [1], gold nanorods [2], gold nanocages [3], gold nanoshells [4]*, etc.* with a diameter between 1-100 nm, have unique localized surface plasmons resonance characteristics [5]. They can selectively absorb the laser energy at a specific wavelength and result in microscale secondary phenomena depending on the pulse duration used, such as photo-thermal conversion, optical breakdown and material fragmentation. The unique photo-thermal properties of gold NP opens the new pathway for nanoscale-mediated temperature and pressure variations, cell apoptosis, drug release, nanosurgery, NP shape modification.

Nanoparticle-mediated laser-induced breakdown (LIB) can be used for NP synthesis [6, 7], cell nanosurgery [8] and laser-induced breakdown spectroscopy (LIBS) [9-11]. Jian *et al.* [12] fabricate ligand free La:$BaSnO_3$ nanocrystal by a 10 ns Nd:YAG laser. They found

* Corresponding authors, e-mails: chenbin@mail.xjtu.edu.cn; dingyingliao@163.com

that embedding those nanocrystals in $BiVO_4$ photoanode matrix could significantly increase the photocurrent density and thus effectively enhance the pulsed electrochemical properties of bismuth tetroxide. Yoshihiko *et al.* [13] showed that gold nanoparticles generated by 1 ns laser irradiation can achieve cells photoperforation, allowing therapeutic exogenous molecules to enter cells. Assion *et al.* [14] measured the distribution of calcium ions (Ca^{2+}) by Fs-LIBS in the inner wall of the cell wall around the stem of sunflower seedlings, and found that Fs-LIBS could analyze and measure biological samples with high spatial resolution.

The NP-mediated LIB mostly use ultrashort intense laser pulses, *e.g.*, nanoor femto-second. Under such ultrashort pulse duration, NP can be fragmented either due to photo-thermal effects or electron emission followed by Coulomb explosion. The fragmentation of gold NP, leads to significant changes in their photo-thermal conversion capabilities [13]. The prevailing effect of fragmentation depends highly on laser parameters. The role of laser parameters, such as the role of pulse duration, is still under discussion. Existing researches are mostly focused on single pulse width nanosecond or femto-second alone. The direct comparisons between the photo-thermal effects and morphological changes induced by two kinds of lasers are rarely deeply investigated.

From the microscopic point of view, it is of great guiding significance to reveal the photo-thermal conversion rules inside gold nanoparticles during nanosecond and femtosecond laser irradiation. At the same time, it is crucial to explore the mechanism of the morphology change of gold nanoparticles under two kinds of laser. To this end, we will present a theoretical model to investigate photo-thermal conversion of gold nanorods in a water medium irradiated by femtosecond and nanosecond lasers with distinct radiant exposure. In addition, combined with the experimental observation, the difference in microscopic NP fragmentation characteristics under two laser pulses will be discussed. Our study provides theoretical guidance for the application of LIB mediated by gold NP, which will be useful to predict the mechanism not only in the laser fragmentation studies but also in laser ablation-based NP production.

Physical model and mathematical description

We use the electron-phonon-two-temperature model to simulate the transient heating process of gold nanorods by ultrafast-pulsed laser [15]. The governing eqs. (1) and (2) describe the transient heating process of free electrons and lattice in gold nanorod under laser radiation, respectively:

$$C_e \frac{dT_e}{d_t} = g(T_l - T_e) + \frac{E_{abs}}{V\tau_p} \tag{1}$$

$$C_l \frac{dT_l}{d_t} = g(T_e - T_l) - \frac{Q_w}{V} \tag{2}$$

where T_e and T_l are the electron and lattice temperatures of the gold nanorods, C_e and C_l – the heat capacities for electrons and the lattice of gold nanorods, d_t – the stands for time interval, V – the volume of the gold nanorods, and τ_p – the laser pulse width. The first terms on the right hand of eqs. (1) and (2) represent the energy coupling between electrons and the lattice. The second terms on the right hand of eqs. (1) and (2) are the laser-heating source and the heat dispersion the surrounding environment, respectively. Among them, g is the coupling factor for calculating heat transfer, E_{abs} – the laser puls energy absorbed by the gold nanorod, which depends on the laser intensity F_{pulse}, and A_{abs} – the absorption cross-sectional area of the gold nanorod:

$$E_{abs} = A_{abs} F_{pulse} \tag{3}$$

when gold nanoparticles exposed to laser light at their plasmonic frequency, the effective absorption cross-section, A_{abs}, is much larger than the geometrical cross-section. The A_{abs} can be calculated by the discrete dipole approximation theory as we illustrated in our previous publication [16], and Q_w is the heat dispersion rate from the gold nanorod to its surrounding environment, which can be calculated:

$$Q_w = A_s G(T_l - T_w) \tag{4}$$

where T_w is the water temperature at the gold nanorod surface, G – the thermal conductance at the gold nanorod/fluid interface, and A_s – the surface area of the gold nanorod. The thermal conductance, G, relates the temperature difference at the interface to the heat flux through the interface, $G = 1.05 \cdot 10^8$ W/m^{2}K [17].

The water temperature, T_w, is can be by calculated by the Fourier heat conduction equation:

$$\rho_w C_{p,w} \frac{\partial T_w}{\partial t} = \frac{\partial}{\partial Z}\left(k\frac{\partial T_w}{\partial Z}\right) + \frac{1}{R}\frac{\partial}{\partial Z}\left(kR\frac{\partial T_w}{\partial Z}\right) \tag{5}$$

where ρ_w is the density of water, $c_{p,w}$ – the specific heat capacity of water, T_w – the temperature of water, and k – the thermal conductivity of water. The energy equations of water and gold nanoparticles are coupled through the thermal conductance, G.

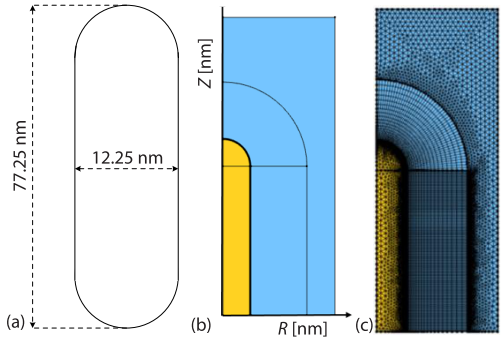

Figure 1. Complete shape of gold nanorods (a), quarter shape (b), and grid distribution (c)

The simulation is conducted based on the software COMSOL. Considering the wavelength of 1064 nm we used in this study, the gold nanorod with an aspect ratio of 6.3 and an effective radius of 12.7 nm has the optimal photo-thermal conversion ability based on our previous finding [16]. Therefore, the size of the gold nanorod used in this study is 77.25 nm × 12.25nm, fig. 1. Considering symmetry, the calculation region is simplified into a 2-D axisymmetric structure with 38.125 nm × 6.125 nm. The meshing of the computational domain is shown in fig. 1(c). The initial temperature of the envi-

Table 1. Thermophysical parameters of water and gold

Parameter	Value
Gold properties	
The electron heat capacity, C_e [Jm^{-3}K^{-1}]	$67.96T_e$
Specific heat of lattice, C_l [Jm^{-3}K^{-1}]	ρ_{gold} *[119+(3.061 · 10^{-2})T_l]
Electron-lattice coupling factor, g [WJm^{-3}K^{-1}]	$2.0 \cdot 10^{16}$
Density, ρ_{gold} [kgm^{-3}]	19300
Enthalpy of fusion, ΔH_{fus} [kJkg^{-1}]	64.0
Thermal conductivity, k_{gold} [Wm^{-1}K^{-1}]	320
Melting temperature, T_m [K]	1337
Water properties at stand conditions	
Density, ρ_w [kgm^{-3}]	1000
Specific heat, $c_{p,w}$ [kJkg^{-1}K^{-1}]	4.184
Thermal conductivity, k [Wm^{-1}K^{-1}]	0.61
Critical temperature, T_{cr} [K]	647

ronment and gold nanorod is 293 K. Neumann boundary condition is used for the surrounding water. A 1064 nm Nd:YAG laser was used in the simulation and two typical laser pulse widths of 100 fs and 7 ns were selected. The thermophysical properties, tab. 1, used in our simulations are from reference [18].

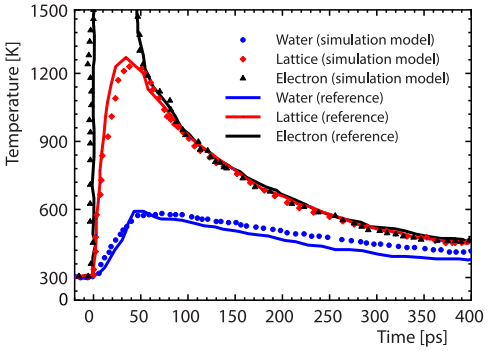

Figure 2. Model validation by comparison between the simulated results with [18]; a 48 nm × 14 nm gold nanorod irradiated by a 760 nm femtosecond laser in water; the pulse width of 250 fs and the pulse energy of 4.7 J/m² are used in our simulation

Simulation results and discussion

Nanorod photo-thermal conversion by ns and fs laser

We first validate our numerical model by comparing simulation results with [18]. Ekici *et al.* [18] simulated the electron and lattice temperatures of a single gold nanorod (48 nm × 14 nm), as well as the surrounding water temperature, irradiated by a 760 nm femtosecond laser. The comparison results are presented in fig. 2. The pulse width of 250 fs and the pulse energy of 4.7 J/m² are used in our simulation, which are consistent with [18]. It can be seen from the fig. 2 that the simulated temperatures of electron, lattice and the surrounding water by this paper are consistent with the results in [18].

The thermal characteristics of gold nanorod irradiated by ultrafast Nd:YAG laser are illustrated in this section. The dynamic temperatures variation of the electron, lattice within gold nanorod and the surrounding water along R (Z = 0) and Z (R = 0) direction are presented in figs. 3(a) and 3(b), respectively. As one can see from the picture, the temperature of electrons and lattice inside the nanogold rod remains uniform. There is a temperature jump at the nanorod/water interface. The water temperature decreased gradually from the nanorod/water interface toward the outer boundary. As we can see from the figure, the temperature of the electron decreases dramatically from 1789 K immediately after laser irradiation 1459 K 30 ps after laser irradiation. On the other hand, the lattice temperature decreased slowly from

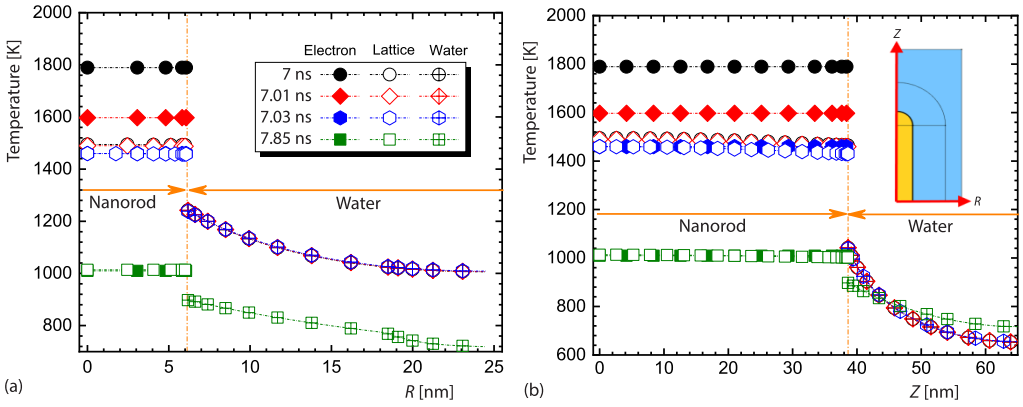

Figure 3. A comparison of the temperature profiles of the electron, lattice within gold nanorod and the surrounding water along *R*-axis (Z = 0) (a) and *Z*-axis (*R* = 0) (b) direction in nanorod centerline immediately after, 0.01 ns after, 0.03 ns after, and 0.85 ns after laser irradiation; the laser radiant exposure: 10 J/m²; the laser pulse duration: 7 ns

1494-1459 K at the same time interval. The thermal equilibrium between the electron and lattice achieves 30 ps after laser irradiation. The water, due to a low thermal diffusivity, keeps its temperature almost unchanged 30 ps after laser irradiation. A substantial water temperature jump was observed 850 ps after laser irradiation. The thermal equilibrium between the nanorod and water achieves 20 ns after laser irradiation.

Using eqs. (1)-(5), the photo-thermal conversion characteristics of gold NP between lasers with different pulse width can be calculated and compared. In this section, two typical laser pulse widths were selected, namely 100 fs and 7 ns.

In this section, we first evaluated the effect of laser radiant exposure on the photo-thermal conversion within nanorod by ns and fs laser. The comparison of temperature profiles of the electron, lattice within gold nanorod and the surrounding water along *R*-axis (a) and *Z*-axis (b) direction in nanorod centerline immediately after 7 ns laser irradiation is illustrated in fig. 4. The laser radiant exposures used in the simulation are 5 J/m^2, 10 J/m^2, and 20 J/m^2, respectively. As we can see from the figure, the temperature of the electron, lattice within gold nanorod and the surrounding water all increased as the radiant exposures increased. After the nanosecond laser irradiation, the water temperature around the gold nanorod increases significantly due to the heat conduction from the nanorod lattice. It can be seen from fig. 4 that the energy threshold of the gold nanorod melting (lattice temperature is higher than the melting point $T_{\text{m.p.}}$) is about 10 J/m^2.

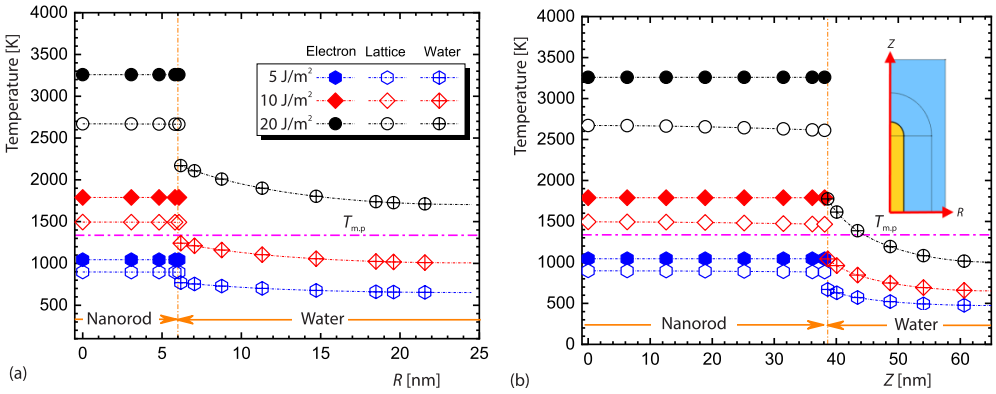

Figure 4. A comparison of temperature profiles of the electron, lattice within gold nanorod and the surrounding water along *R*-axis (Z = 0) (a) and *Z*-axis (*R* = 0) (b) direction in nanorod centerline immediately after laser irradiation; horizontal line in the figure represent melting point of bulk gold $T_{\text{m.p}}$; the laser radiant exposure: 5, 10, and 20 J/m^2; the laser pulse duration: 7 ns

We also investigated the nanorod photo-thermal conversion by fs laser irradiation. The temperature profiles of the electron, lattice within gold nanorod and the surrounding water along *R*-axis (a) and *Z*-axis (b) direction in nanorod centerline immediately after 100 fs laser irradiation is illustrated in fig. 5. The laser radiant exposures used in the simulation are 0.2 J/m^2, 0.5 J/m^2, and 1 J/m^2. As the incident radiant exposure increases, the temperature of the electron, lattice within gold nanorod and the surrounding water all increase. As can be seen from the fig. 5, the photo-thermal conversion characteristic of nanorod irradiated by fs is obviously different from that of ns laser irradiation. During the fs laser irradiation, a strong thermal non-equilibrium is observed. The temperature of electron is much higher than that of lattice and surrounding water. The electron temperature exceeds the Coulomb explosion threshold $T_{\text{c.e.}}$ at the radiant exposure of 0.5 J/m^2. It can also be found from the simulation that the melting threshold of the gold nanorod under femtosecond laser irradiation (approximately 0.5 J/m^2) is greatly lower than that under nanosecond laser irradiation (approximately 10 J/m^2).

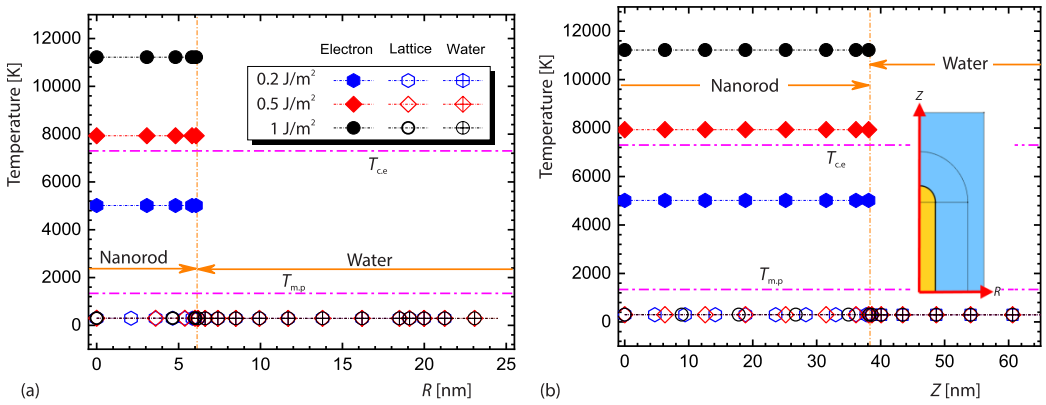

Figure 5. A comparison of temperature profiles of the electron, lattice within gold nanorod and the surrounding water along *R*-axis (*Z* = 0) (a) and *Z*-axis (*R* = 0) (b) direction in nanorod centerline immediately after laser irradiation; horizontal lines in the figure represent melting point of bulk gold $T_{m.p}$ and threshold for the Coulomb explosion $T_{c.e}$, respectively; the laser radiant exposure: 0.2 J/m², 0.5 J/m², and 1 J/m²; the laser pulse duration: 100 fs

Compared to fig. 4, the temperature differences between the lattice and free electrons and between lattice and surrounding water by fs laser irradiation is significantly larger than the case in ns laser irradiation. Furthermore, due to less heat conduction in fs pulse duration, the water temperature is almost unaffected by laser irradiation. This trend can be further illustrated in fig. 6, which presents a comparison of normalized temperature profiles of the electron, lattice within gold nanorod and the surrounding water immediately after 7 ns and 100 fs laser irradiation. The laser radiant exposure of 10 J/m² for 7 ns and 0.5 J/m² for 100 fs laser, which are the thresholds for nanorod melting for two laser pulse durations, respectively. It can be seen clearly from fig. 6 that the relative lattice and water temperature to the electron by the ns laser irradiation is much higher than that of fs laser irradiation due to higher heat dispersion from electron lattice and to the surrounding water in a relative longer pulse duration.

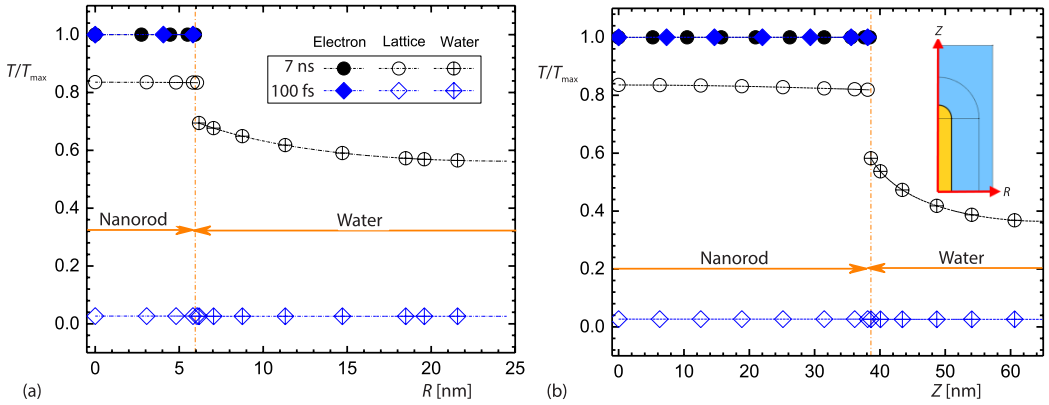

Figure 6. A comparison of normalized temperature profiles of the electron, lattice within gold nanorod and the surrounding water along *R*-axis (*Z* = 0) (a) and *Z*-axis (*R* = 0) (b) direction in nanorod centerline immediately after 7 ns and 100 fs laser irradiation; the T_{max} represents the maximum temperature of electron by ns or fs laser irradiation; the laser radiant exposure: 10 J/m² for ns laser and 1 J/m² for fs laser

Nanorod fragmentation by ns and fs laser

Figure 7 shows dynamic temperature variation of electron, lattice within gold nanorod and the surrounding water irradiated by ns 7(a) and fs 7(b) laser. The laser radiant exposure of 10 J/m^2 and 1 J/m^2 is used for 7 ns and 100 fs laser, respectively. Here, we see the remarkable effect of pulse duration the temperature dynamics. Electron, lattice and water (at nanorod/water interface) temperature increase almost synchronously during the ns laser irradiation, fig. 7(a). The water temperature reaches boiling point at the time instant of $t_{b.p}$ = 1.2 ns. The lattice temperature reaches the melting point at the time instant of $t_{m.p}$ = 5.3 ns. Most significantly, electron temperatures of about 7300-8200 K to exceed the Coulomb explosion threshold can never be reached before $t_{b.p}$ and $t_{m.p}$ by ns laser irradiation. Consequently, the fragmentation of the nanorod is more likely due to particle melting, while the Coulomb explosion is unlikely occur in the nanosecond laser irradiation.

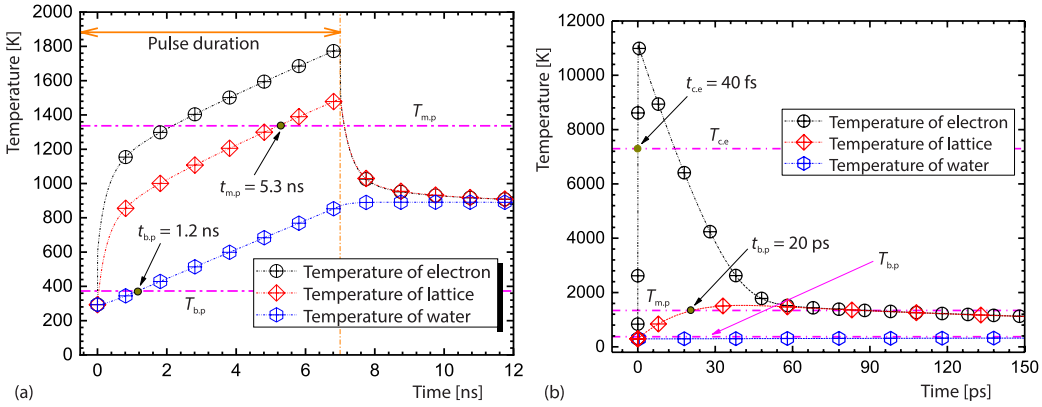

Figure 7. Dynamic temperature variation of electron, lattice within gold nanorod and the surrounding water irradiated by; (a) nanosecond laser irradiation (nanorod fragmentation by melting) and (b) femtosecond laser irradiation (nanorod fragmentation by Coulomb explosion) laser; horizontal lines in the figure represent boiling poring of water $T_{b.p}$, melting point of bulk gold $T_{m.p}$ and threshold for the Coulomb explosion $T_{c.e}$, respectively; the laser radiant exposure: 10 J/m^2 for 7 ns laser, 1 J/m^2 for 100 fs laser)

In contrast to the fs laser irradiation, electron temperature rises instantaneously reaching a maximum value of at the end of fs laser irradiation and then decreases, fig. 7(b). Subsequently, the energy deposited into the electronic system transferred via electron-phonon-coupling to the lattice system, leading to a rise of lattice temperature up to its maximum of 1527 K within 40 ps. Then, at approximately 70 ps, electron and lattice reach their thermal equilibrium and the nanorod starts to cool down in the following several hundreds of picoseconds through heat dissipation the surrounding water. The electron temperature reaches the Coulomb explosion threshold about 7300-8200 K at the time instant of $t_{c.e}$ = 40 fs, while the lattice temperature reaches the melting point at the time instant of $t_{m.p}$ = 20 ps. Therefore, the Coulomb explosion mechanism is highly likely to occur because $t_{c.e}$ is earlier than $t_{m.p}$.

We also conducted nanorod laser irradiation experiment to further prove our numerical simulation. In order to illustration the melting and Coulomb explosion process of gold nanorods by ns and fs laser irradiation, we firstly carried out an experimental observation on the photo-thermal effect induced by ns laser on nanorod. In our experiment, 1064 nm Nd: YAG laser with a pulse width of 7 ns is used, which is consistent with the calculation. The laser spot diameter is 2 mm and the incident laser radiant exposure is 0.6 J/cm^2, 3 J/cm^2, 6 J/cm^2,

14 J/cm^2, and 20 J/cm^2, respectively. The gold nanorods were prepared by the seed growth method containing $AgNO_3$ as we illustrated in our previously publication [16]. The nanorod morphology before and after irradiation were examined by transmission electron microscopy (TEM, JEOL2100, Japan).

Figure 8 shows the TEM images of gold nanorods before and after ns laser irradiation with different radiant exposure. It can be seen from fig. 8(a), the prepared nanarod with the average size of 77.25 nm × 12.25 nm which is consistent with our simulation. We can also see from figs. 8(b)-8(f) that as the laser incident radiant exposure increases, the ns laser irradiation causes the melting of the surface of the gold nanorods into gold nanospheres with equal volume, fig. 8(e). When the laser energy density continues to increase, the gold nanospheres will melt into smaller spherical particles, fig. 8(f).

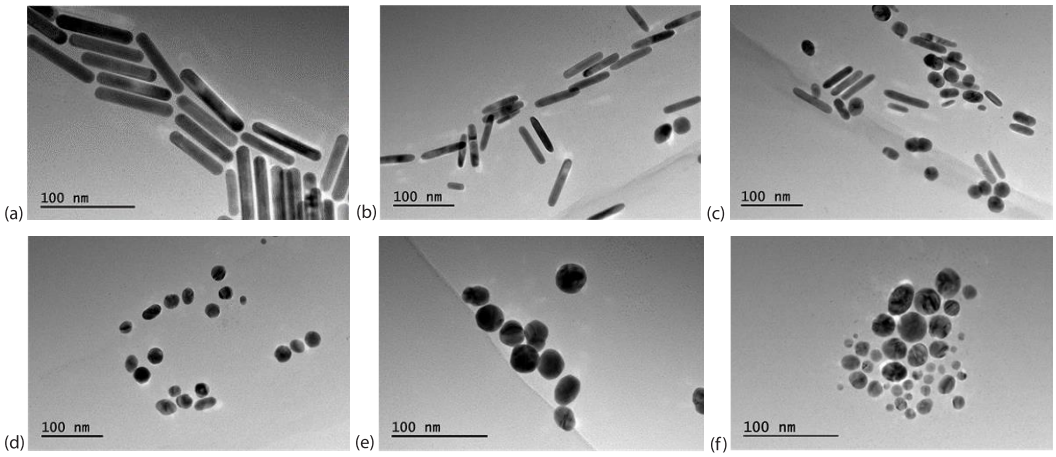

Figure 8. The TEM images of gold nanorods before and after ns Nd:YAG laser irradiation with different radiant exposure; (a) before, (b) 0.6 J/cm^2, (c) 3 J/cm^2, (d) 6 J/cm^2, (e) 14 J/cm^2, and (f) 20 J/cm^2

We compare our ns laser irradiation experiment results to the published fs laser irradiation by Link *et al.* [15]. In their experiment, a laser with a wavelength of 800 nm and a pulse width of 7 ns and 100 fs were used, respectively. The gold nanorods were prepared by electrochemical method as shown in [19]. The morphology of the prepared gold nanorods were characterized by TEM before and after irradiation. The laser parameters used in the aforementioned experiments are the same as those in the simulation in this paper. The experiment results in fig. 9 shows that after the fs laser irradiation the gold nanorods change their morphology under a lower laser incident radiant exposure of 0.001 J/cm^2. When the laser radiant exposure increases, irregular spheres with sharp angles and raised edges were observed, which is mainly caused by the Coulomb explosion by fs laser irradiation. This phenomenon was significantly different from that by nanosecond laser irradiation, fig. 8. When the laser radiant exposure continues to increase, the irregular gold nanoparticles continue to be broken into smaller powder.

In this study, the laser incident radiant exposure used in the experiment is higher than the simulation results. On the one hand, the energy dissipation caused by the laser passing through the aqueous solution was not considered in the simulation, on the other hand, the laser acted on the nanoparticle group in the experiment, and the laser energy density requirement was obviously higher than that of the single particle. The comparison between figs. 8 and 9 shows that the mechanism of nanorods forming gold nanospheres under femtosecond and nanosecond laser irradiation is different. This difference can be preliminarily explained based on the sim-

ulation results in this article. It can be seen from figs. 5-7 that when the 0.5 J/m^2 femtosecond laser irradiates the laser nanogold rods, the nanogold rods will melt when they reach the melting threshold, but at this time, the water temperature around the nanogold rods is much lower than the melting temperature of the gold rods. The temperature difference at the interface with water is as high as 7580 K. Such a large temperature difference causes that the surface and the inside of the gold nanorods cannot undergo thermal expansion and volume change at the same time. The difference in the volume changes of each part leads to the formation of huge internal stress, which causes the gold nanorods to easily produce point defects and line defects from the inside, and then evolve into planar defects, and then break. When the 10 J/m^2 nanosecond laser acts on the gold nanorods and reaches the melting threshold, the water temperature around the gold nanorods is equivalent to the melting temperature of the gold rods, and the temperature difference at the interface between the gold nanorods and water is 625 K, which is much lower than the case of femtosecond laser heating. At this time, the thermal stress on the surface of the gold nanorods is significantly reduced and it is not easy to break, so the gold nanospheres are mainly formed by thermal melting.

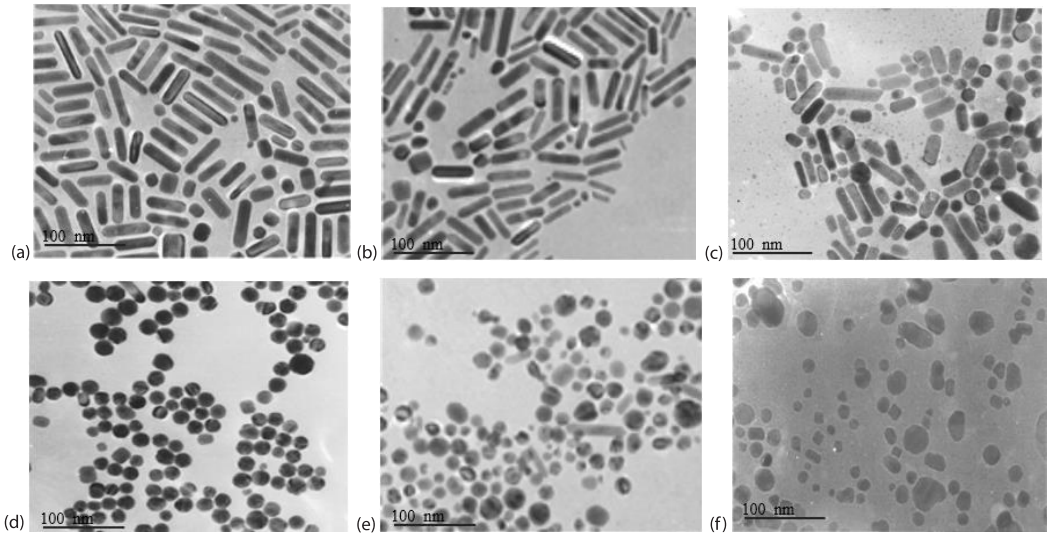

Figure 9. The TEM images of gold nanorods irradiated by femtosecond laser with different laser energy densities [15]; (a) before, (b) 0.0002 J/cm^2, (c) 0.001 J/cm^2, (d) 0.25 J/cm^2, (e) 0.56 J/cm^2, and (f) 10.2 J/cm^2

Conclusion

In this paper, theoretical and experimental studies have been carried out to analyze the photo-thermal conversion inside and near gold nanoparticles during ultrashort laser irradiation. The results show that the temperature difference between the lattice and the free electron in the gold nanorod is significantly reduced by nanosecond laser irradiation compared to femtosecond laser irradiation. The melting threshold for gold nano rods (about 0.5 J/m^2) by the femtosecond laser irradiation is 20 times lower than that of the nanosecond laser irradiation (about 10 J/m^2). The gold nanorod fragment mechanism caused by nano and femto second laser irradiation is greatly different: particle melting is more likely to occur in nanosecond laser irradiation, while the Coulomb explosion is highly likely to occur in femtosecond laser irradiation. This finding is also supported by our experimental observation: the gold nanorods melted into the smaller

particles under nanosecond laser irradiation, while gold nanorods broke down into smaller irregular particles with sharp edges. The results presented in this paper have important guiding significance for high intensity pulsed laser ablation of metal nanoparticles.

Acknowledgment

This study was funded by the National Natural Science Foundation of China (No. 51976170, 51727811).

References

[1] Lv, H, *et al*., Mesoporous Gold Nanospheres Via Thiolate-Au (I) Intermediates, *Chemical Science*, *10* (2019), 26, pp. 6423-6430
[2] Ruff, J., *et al*., Multivalency of PEG-thiol Ligands Affects the Stability of NIR-absorbing Hollow Gold Nanospheres and Gold Nanorods, *Journal of Materials Chemistry B*, *4* (2016), 16, pp. 2828-2841
[3] Sun, H. P, *et al*., Cancer Cell Membrane-Coated Gold Nanocages with Hyperthermia-Triggered Drug Release and Homotypic Target Inhibit Growth and Metastasis of Breast Cancer, *Advanced Functional Materials*, *27* (2017), 3, 1604300
[4] Shabaninezhad, M., Ramakrishna, G., *et al*., Theoretical Investigation of Size, Shape, and Aspect Ratio Effect on the LSPR Sensitivity of Hollow-Gold Nanoshells, *Journal of Chemical Physics*, *150* (2019), 14, 144116
[5] Ghosh, S. K., Pal, T., *et al*., Interparticle Coupling Effect on the Surface Plasmon Resonance of Gold Nanoparticles: From Theory to Applications, *Chemical Reviews*, *107* (2007), 11, pp. 4797-4862
[6] Patil, P. P., et al., Pulsed-Laser-Induced Reactive Quenching at Liquid-Solid Interface: Aqueous Oxidation of Iron, *Physical Review Letters*, *58* (1987), 3, 238
[7] Aguirre, C. M., *et al*., Laser-Induced Reshaping of Metallodielectric Nanoshells under Femtosecond and Nanosecond Plasmon Resonant Illumination, *Journal of Physical Chemistry B*, *108* (2004), 22, pp. 7040-7045
[8] Boutopoulos, C., *et al*., Cell Perforation Mediated by Plasmonic Bubbles Generated by a Single Near Infrared Femtosecond Laser Pulse, *Journal of Biophotonics*, *9* (2016), 1-2, pp. 26-31
[9] Lithgow, G. A., *et al*., Ambient Measurements of Metal-Containing PM 2.5 in an Urban Environment Using Laser-Induced Breakdown Spectroscopy, *Atmospheric Environment*, *38* (2004), 20, pp. 3319-3328
[10] Gallou, G., Aerosols Analysis by LIBS for Monitoring of Air Pollution by Industrial Sources, *Aerosol Science and Technology*, *45* (2011), 8, pp. 918-926
[11] Kwak, J. H., Determination of Heavy Metal Distribution in PM10 During Asian Dust and Local Pollution Events Using Laser Induced Breakdown Spectroscopy (LIBS), *Aerosol Science & Technology*, *46* (2012), 10, pp. 1079-1089
[12] Jian, J., *et a*l., Embedding Laser Generated Nanocrystals in BiVO4 Photoanode for Efficient Photoelectrochemical Water Splitting, Nature Communications, *10* (2019), 2609
[13] Yoshihiko, A., *et al*., Laser-Induced Breakdown of an Optically Trapped Gold Nanoparticle for Single Cell Transfection, *Optics Letters*, *38* (2013), 17, pp. 3402-3405
[14] Assion, A., *et al*., Femtosecond Laser-Induced-Breakdown Spectrometry for Ca^{2+}Analysis of Biological Samples with High Spatial Resolution, *Applied Physics B: Lasers & Optics*, *77* (2003),4, pp. 391-397
[15] Link, S., *et al*., Laser-Induced Shape Changes of Colloidal Gold Nanorods Using Femtosecond and Nanosecond Laser Pulses, *The Journal of Physical Chemistry B*, *104* (2000), 26, pp. 6152-6163
[16] Xing, L., *et al*., Enhancement of Light Absorption by Blood to Nd: YAG Laser Using PEG-Modified Gold Nanorods, *Lasers in Surgery & Medicine*, *48* (2016), 8, pp. 790-803
[17] Plech, A., *et al*., Laser-Induced Heating and Melting of Gold Nanoparticles Studied by Time-Resolved x-Ray Scattering, *Physical Review B*, *70* (2004), 19, pp. 3352-3359
[18] Ekici, O., *et al*., Thermalanalysis of Gold Nanorods Heated with Femtosecond Laser Pulses, *Journal of Physics D: Applied Physics*, *41* (2008), 18, 185501
[19] Hu, X. J., *et al*., Gold Nanorods – From Controlled Synthesis and Modification NanoBiological and Biomedical Applications, *Acta Physico-Chimica Sinica*, *33* (2017), 7, pp. 1324-1337

Paper submitted: August 28, 2021
Paper revised: October 8, 2021
Paper accepted: October 14, 2021